Journal of Petroleum Science and Engineering 214 (2022) 110502

Contents lists available at ScienceDirect

Journal of Petroleum Science and Engineering

journal homepage: www.elsevier.com/locate/petrol

Sorptive permeability loss determined from strain-based analysis of tightly constrained experiments on shale

Brandon Schwartz *, Derek Elsworth

Department of Energy and Mineral Engineering and G3 Center, Penn State University, University Park, PA, USA

ARTICLE INFO

Keywords:
Sorptive permeability evolution
Sorptive strain
Shale

ABSTRACT

We build a model to determine sorptive permeability loss from observed total permeability evolution by considering adsorption and poromechanical expansion as parallel processes. The model is cross verified with a separately derived strain-based model for sorptive permeability evolution. Both models are compared to laboratory data and are shown to have excellent agreement. We isolate the sorptive strain from the total strain measured during serial injection of sorptive then non-sorptive gas species. Our model predicts that injection of a non-sorptive gas into a shale saturated with a sorptive gas causes permeability to approximately double in both the bedding-parallel and bedding-perpendicular directions. We preform nitrogen floods at constant stress, pore pressure, and temperature to observe the sorptive permeability recovery absent other confounding effects. We confirm that in shales the component of permeability evolution due to sorptive swelling can be isolated from effective stress effects. Laboratory results show a 206% and a 234% permeability increase in the bedding-perpendicular and bedding-parallel directions, respectively, as a result of nitrogen flooding. This counters and indeed dominates over any sorptive permeability loss that despite a modest fraction of organic material (~1–2%) is amplified by the low pore density. We find that sorptive permeability evolution in shales is controlled by the sorptive strain, pore density, and pore geometry.

1. Introduction

Shale is a sedimentary rock typified by strongly anisotropic transport and mechanical properties (Sone and Zoback, 2013; Schwartz et al., 2019a). Within the matrix, individual mineral components of silica, calcite, organic matter, and clays form thin laminae separated by fracture planes which allow for greater fluid flow parallel to bedding (Bandyopadhyay, 2009; Crook et al., 2002; Bonnelye et al., 2017). These bedding features are observed to cause brittle failure planes when coring (Heng et al., 2020; Lyu et al., 2015). Porosity is concentrated between laminae as micro-fissures that create a set of preferential flow paths throughout the shale (Keller et al., 2011; Yan et al., 2015).

1.1. Adsorption in shales

Many shales experience adsorption in the presence of hydrocarbons, particularly methane. Adsorption in shales can account for up to half of the gas storage—in the case of low organic content, illite may be responsible for the additional sorptive storage (Lu et al., 1995). Adsorption in the organic matter causes shales to internally swell, constricting flow paths and reducing permeability (Izadi et al., 2011). Concurrently, increasing the pore pressure of any gas causes poromechanical expansion, leading to increased permeability. Bulk expansion due to sorptive swelling is additive with poromechanical expansion whereas permeability evolution is competitive due to these strains (Harpalani and Chen, 1997; Cui and Bustin, 2005; Robertson and Christiansen, 2007; Mazumder and Wolf, 2008; Siriwardane et al., 2009).

Sorptive swelling occurs along the surface of the adsorbent. In the presence of any appreciable amount of gas, swelling is essentially isotropic (Robertson, 2005; Robertson and Christiansen, 2006). However, because shale is a mechanically transversely isotropic material each of the three principal components of the sorptive strain primarily impacts only one of the two directional permeabilities. The orthogonal impact of each component of the sorptive strain is captured through the Poisson effect. As such, three-dimensional models of permeability evolution in shale can be reduced to two dimensions without loss of model fidelity (Schwartz et al., 2019b).

* Corresponding author.
E-mail address: schwartz@psu.edu (B. Schwartz).

https://doi.org/10.1016/j.petrol.2022.110502
Received 4 January 2021; Received in revised form 7 April 2022; Accepted 8 April 2022
Available online 14 April 2022

1.2. Competing processes in permeability evolution

Fig. 1 illustrates that pores in shale are concentrated between bedding planes and can be characterized using pore spacing *s*, pore aperture *b*, and pore length *a*. Fig. 1a shows an idealized pore surrounded by matrix rock including organic matter (OM). With increasing pore pressure, the pore expands due to the traction along the pore boundary (Fig. 1b). Increasing pore size also causes bulk expansion of the core. If the gas species is sorptive, then an additional deformation occurs as the surrounding organic matter swells (Fig. 1c). Because the deformation originates outside of pores, it creates a separate bulk expansion that concurrently constricts flow paths by causing pore closure. Combining these mechanisms, increasing pore pressure with a sorptive species causes pore aperture to increase due to poromechanical expansion and to simultaneously decrease due to sorptive swelling (Fig. 1d). If the injection pressure of a sorptive gas is higher than the equilibrium pore pressure, poromechanical expansion of the pore space competes with the permeability reduction caused by sorptive swelling (Liu et al., 2010; Kumar et al., 2016). At any given pore pressure, the bulk expansion from a sorptive gas is larger than that from a non-sorptive gas because the sorptive swelling causes an additional deformation.

This ensemble response to sorptive gases can be further illustrated in Fig. 2. In Fig. 2a, strain is plotted against increasing pore pressure with expansion shown as positive strain. The sorptive strain follows a Langmuir-type curve that grows quickly at low pore pressure and slows as it approaches a maximum strain at higher pore pressure. After 100% of the available adsorption sites are filled, there is no further sorptive strain. Instead, additional pore pressure only causes additional pore expansion. The total strain curve will be the sum of the sorptive strain and the poromechanical strain. Fig. 2b illustrates that the net pore response will be positive or negative depending on whether sorptive pore closure is larger than mechanical pore expansion. At lower pore pressures, the pore closure caused by sorptive swelling is larger than the pore expansion caused by increased pore pressure. At larger pore pressures, incremental poromechanical expansion outpaces incremental sorptive swelling and the net pore response is expansion. Fig. 2c translates the net pore response to a net permeability response. At low pore pressures, permeability decreases due to the dominant effect of sorptive swelling. As the rate of permeability reduction due to Langmuir swelling decreases, the rate of permeability enhancement due to poromechanical expansion increases. At higher pressures, permeability can increase beyond the initial permeability as poromechanical expansion becomes the dominant effect. Therefore, there is a point at which poromechanical expansion outpaces Langmuir swelling and permeability reduction reaches an inflection point to become permeability enhancement.

1.3. Permeability models for sorptive media

Shale and coal are both fractured, sorptive media and their responses to sorptive gases are similar (Kumar et al., 2016). Many permeability models have been developed to capture the effect of sorption in coals (Seidle et al., 1992; Palmer and Mansoori, 1996; Cui and Bustin, 2005; Shi and Durucan, 2005; Palmer, 2009), and permeability evolution in fractured, sorptive media is typically cast in terms of evolving strains (Liu et al., 2011). These strains occur due to organic swelling within the matrix and sorption within flow channels (Li et al., 2017). In flow channels composed of sorptive minerals, the layer of adsorbed gas against the flow channel wall directly reduces the flow channel aperture (Sakhaee-Pour and Bryant, 2012). Conversely, the shrinkage of organic matter during desorption increases pore aperture (Levine, 1996; Liu and Rutqvist, 2010). The magnitude of permeability reduction caused by sorptive swelling represents the potential permeability enhancement in the event of desorption. In coals, methane desorption has been shown to increase permeability 2- to 5-fold (Harpalani and Schraufnagel, 1990). This has been directly observed in coal basins where permeability increased during depletion as organic shrinkage expanded fractures, which had a larger effect than the additional compression caused by the overburden stress (Mavor and Vaughn, 1998).

Permeability evolution in shales depends on pore geometry, pore density, and pore stiffness (Schwartz et al., 2019c). Pore geometry is captured by the aspect ratio b/a, where *b* is the pore aperture and *a* is the pore length (Fig. 1a). Pore density can be quantified using the spacing-to-aperture ratio s/b as a proxy—larger values of s/b correspond to a lower pore density. Pore stiffness is influenced by the minerals immediately surrounding the pore, although pores are typically geometrically much softer than the surrounding matrix. Sorptive permeability evolution is also driven by the amount of total organic

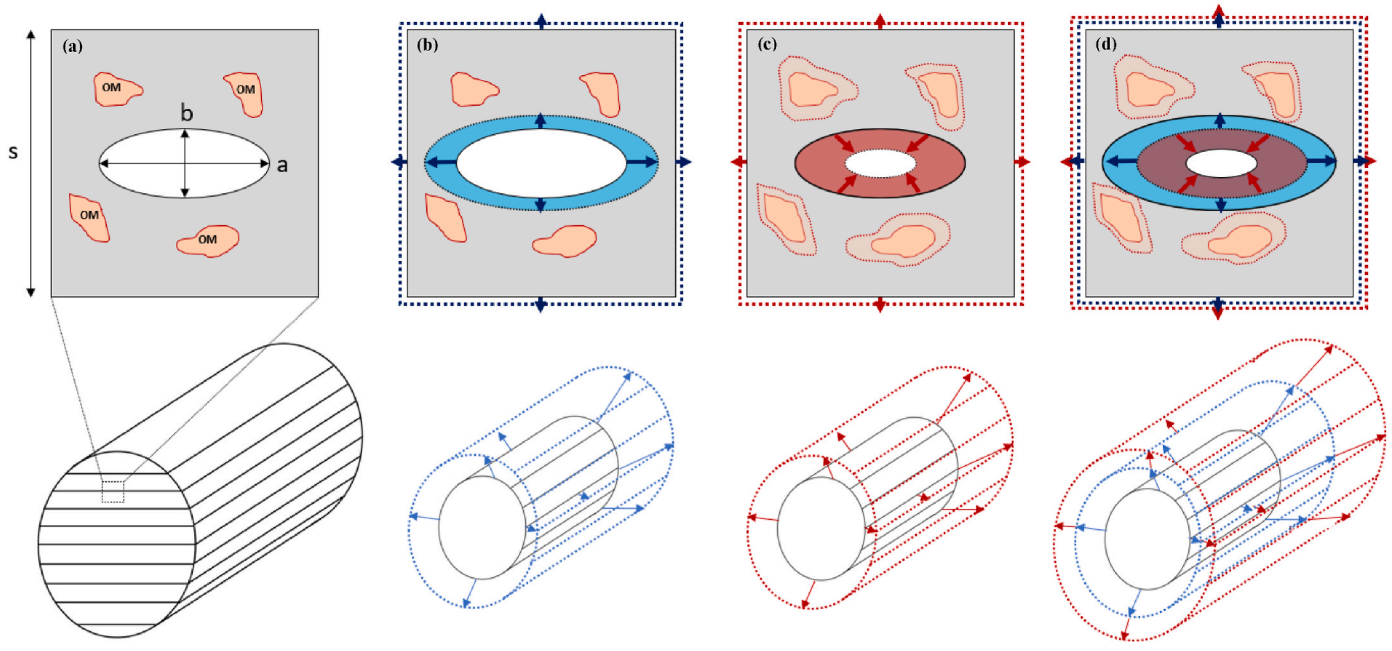

Fig. 1. Diagram of parallel processes occurring in fissure-like ellipsoid pores in shale core. Fig. 1b shows poromechanical expansion, Fig. 1c shows sorptive swelling, and Fig. 1d shows their combined effect.

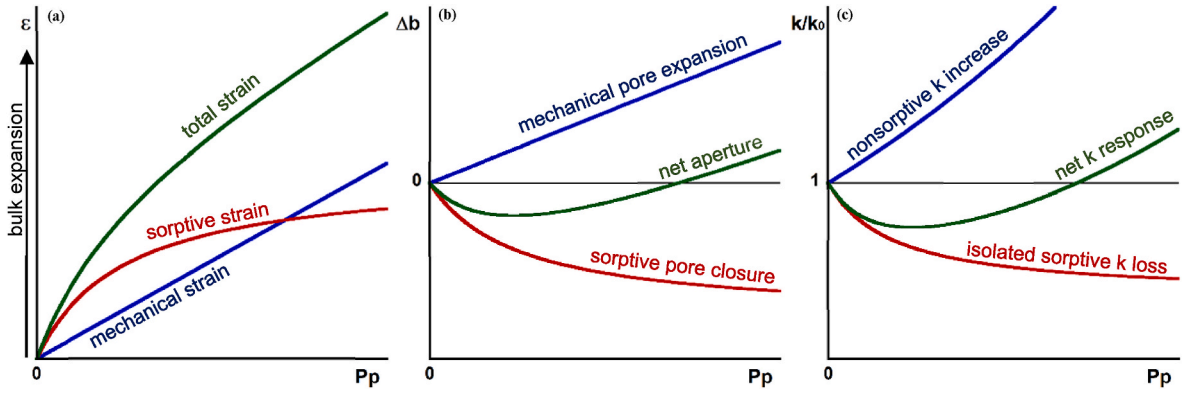

Fig. 2. Competitive response in pore deformation due to sorptive and nonsorptive processes.

carbon (%TOC) available for adsorption. In this regard the main difference between coals and shales is the %TOC, with many shales typified by lower %TOC and many coals having 90–99% TOC. The %TOC is the primary influence on the magnitude of the sorptive strain, which in coals can be 10^{-2} (Zhang et al., 2008; Robertson, 2008) and in shales 10^{-4}. However, permeability loss is often comparable. This study addresses this disparity—that a smaller sorptive strain in shales can produce a similar permeability reduction. We propose that the relative pore density must be low in shales to accommodate for the similar permeability evolution. We build strain curves to isolate the sorptive strain and test the role of pore density with a strain driven model for permeability evolution. We verify our model using nitrogen flooding to demonstrate that relaxing the sorptive strain increases the matrix permeability of shales.

2. Methods

We conduct two sets of experiments on samples of Marcellus shale, a Middle Devonian black shale characterized by siliciclastic input from the Alleghanian Orogeny. The mineral composition of the interval of the Marcellus that samples were cored from is approximately 38% silicates, 50% clays (predominantly illite and smectite), 9% carbonates, and 3% TOC by volume. Core samples are from a well drilled in the northern part of West Virginia. We first conduct a suite of experiments designed to capture the sorptive strain evolution and related sorptive permeability evolution. With this information, we design an experiment that isolates sorption-driven permeability evolution via nitrogen flooding at constant pore pressure. Nomenclature is summarized in Table 1.

Table 1
Nomenclature.

Symbol	Description	Units
a	Pore length	m
A	Cross-sectional area	m^2
b	Pore aperture	m
E	Elastic modulus	GPa
k	Permeability	m^2
L	Sample length	m
P	Pore pressure	MPa
P_L	Langmuir pressure	MPa
s	Pore spacing	m
V_{up}	Upstream reservoir volume	m^3
V_{dn}	Downstream reservoir volume	m^3
α	Pressure decay rate	s^{-1}
β	Gas compressibility	Pa^{-1}
ε	Strain	–
μ	Gas viscosity	Pa·s
ν	Poisson's ratio	−/−
σ	Applied stress	MPa

2.1. Sorptive strain experiment

Experiments are conducted in a triaxial vessel loaded with cores of Marcellus shale (Fig. 3) at 21 °C. For the first experiment, we allow a sample to compact and we measure permeability at different pore pressures and constant temperature. We start with helium and then repeat the experiment with methane. We use a linear variable differential transformer (LVDT) throughout the experiments to record longitudinal displacement. Because the sorptive strain and poromechanical strain act concurrently and in parallel at any given location, the methane experiment captures the additive effect whereas the helium strain captures the poromechanical effect only. Therefore, the helium strain curve can be subtracted from the methane curve to recover the sorptive strain.

2.2. Methane desorption experiment

The second experiment floods three methane saturated shale cores with nitrogen. Nitrogen is a slightly sorptive gas, and results will include a minor influence from the sorptive strain of nitrogen. However, nitrogen is a plentiful and inexpensive gas that is already used in field-scale flooding for enhanced gas recovery, which is why we select it over a completely nonsorptive gas like helium. Trials are conducted on two samples cored in the bedding-parallel direction (19 × 16mm) and one in the bedding-perpendicular direction (19 × 3mm). Experiments are conducted at 21 °C. The stress state of the bedding-parallel floods is 24 MPa hydrostatic external stress and 6 MPa pore pressure. The stress state of the bedding-perpendicular flood is dropped to 10 MPa external hydrostatic stress and 6 MPa pore pressure in order to obtain a permeability measurement. Each sample is saturated with methane at 6 MPa pore pressure. After initial permeability measurements, the upstream gas lines are evacuated and vacuumed to remove all methane. This process is limited to 5 min in order to minimize gas leaving the sample on the upstream side. Once the lines are evacuated, nitrogen is injected into the upstream side while the downstream lines retain methane at 5.7 MPa. The upstream line pressure is raised to 6.3 MPa and the pressure pulse test is repeated with nitrogen infiltrating the sample from the upstream side and methane produced on the downstream side. This process is repeated daily until there is no more change in permeability. We use pressure pulse tests (Brace et al., 1968) to solve for permeability from the pressure decay, $\alpha = ln(dp)/dt$, as:

$$k = \frac{\alpha\mu\beta L}{A}\frac{V_{up}V_{dn}}{V_{up}+V_{dn}}. \quad (1)$$

where μ is gas viscosity and β is isothermal gas compressibility, both calculated using 21 °C and 6 MPa. Upstream and downstream reservoir volumes are 5.96 × 10^{-6} m^3 and 3.71 × 10^{-6} m^3, respectively.

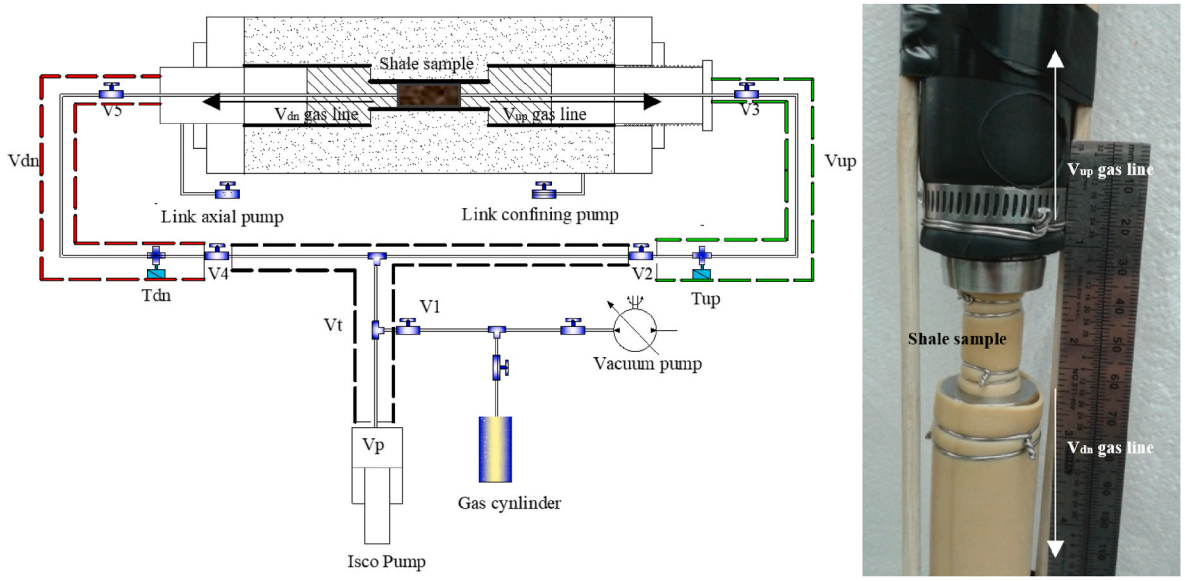

Fig. 3. Schematic of triaxial vessel. The shale sample is housed in a water-tight jacket and placed in the vessel. Upstream and downstream gas volumes can be isolated from each other to calculate pressure pulse decay. An LVDT is mounted to the outside of the vessel.

3. Results

We resolve the strain data in order to isolate the sorptive strain. We also isolate the sorption-only permeability evolution of the first set of experiments. Upon relaxing the sorptive strain present at a selected pore pressure of 6 MPa, we observe an increase in permeability that matches the permeability increase predicted to result from nitrogen flooding at constant pore pressure.

3.1. Resolving sorptive strain

We plot strain versus pore pressure for flooding by first helium then replacing with methane in Fig. 4. The resolution of the LVDT is 0.1 μm with smaller displacement rounded to the nearest 0.1 μm. Because the lengths of our samples are on the order of millimeters, a strain of 10^{-4} is the minimum resolvable increment. Strains less than 0.1 μm are automatically rounded by the LVDT. We have included boundaries in Fig. 4 to show the possible range of strains that could be obscured by the limits of resolution of the LVDT. In the case of methane injection, the measured strain is the sum of the poromechanical expansion and the sorptive swelling:

$$\varepsilon_{tot} = \varepsilon_p + \varepsilon_s \tag{2}$$

such that

$$\varepsilon_s = \varepsilon_{tot} - \varepsilon_p \tag{3}$$

where

$$\varepsilon_s = \varepsilon_L \frac{P}{P + P_L} \tag{4}$$

The methane strain data represent ε_{tot} as both strains are present at increasing pore pressure. The helium strain curve represents poromechanical expansion only and is equal to ε_p. In order to find ε_s, we subtract the helium-induced strain from the methane-induced strain at each pressure and fit the resulting data to a Langmuir-type strain curve according to Eq. (4). From the plot below, the sorptive strain at 6 MPa is 1.15×10^{-4}, which can be used to calculate P_L and ε_L.

Using Eq. (3) and Eq. (4), the Langmuir strain can be isolated. The strain data in Fig. 4 are used as input into Eq. (3) and a Langmuir strain curve is fit to the result using Eq. (4). Results for the isolated sorptive

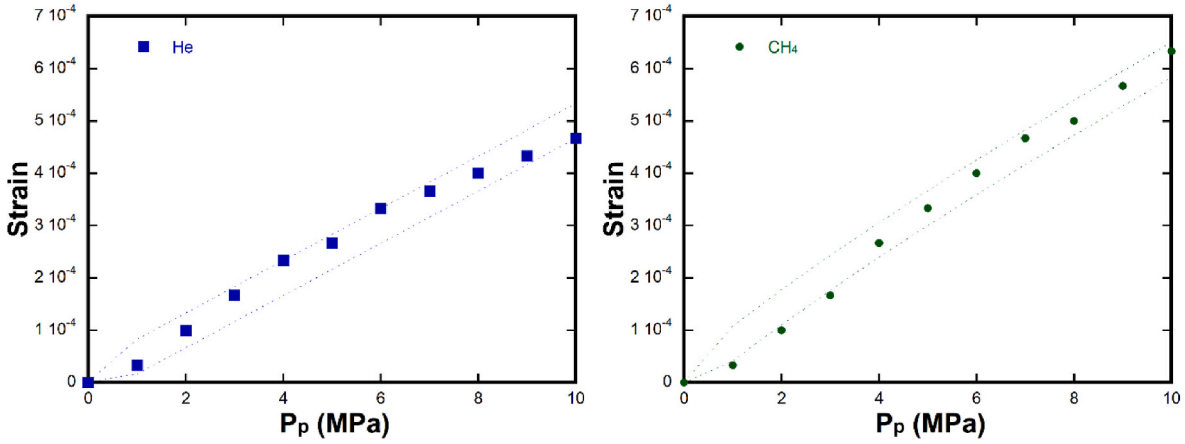

Fig. 4. Strain vs. pore pressure for helium (left) and methane (right). The blue and green dotted lines show measurements ± 0.1 μm of a linear fit to the strain data in order to illustrate the range of strain values that could be obscured by the LVDT's resolution. (For interpretation of the references to colour in this figure legend, the reader is referred to the Web version of this article.)

strain are plotted in Fig. 5. At low pressures, the lower than expected measurements of strain for methane suggest that the core may not have been fully saturated, although the strain data are within the margin of error for the LVDT. In Eq. (4), a Langmuir pressure P_L of 7 MPa and a Langmuir strain ε_L of 2.75×10^{-4} provide an excellent fit to Eq. (3).

3.2. Solving for sorption-induced permeability evolution

When considering methane permeability evolution with increasing pore pressure, the poromechanical strain and the sorptive strain are parallel processes creating a net response at each location in the matrix. The permeability evolution can be modeled as processes in parallel as (Wang et al., 2012):

$$\frac{k}{k_o} = \left(1 + \left(\frac{s}{b_o} + \frac{a(1-\nu)}{b_o}\right)(\varepsilon_p + \varepsilon_s)\right)^3 \tag{5}$$

We group the variables in Eq. (5) into sorptive and non-sorptive components:

$$\frac{k}{k_o} = (1 + A - B)^3 \tag{6}$$

$$A = \frac{\Delta b_p}{b_o} = \left(\frac{s}{b_o} + \frac{a(1-\nu)}{b_o}\right)\varepsilon_p = \left(\frac{s}{b_o} + \frac{a(1-\nu)}{b_o}\right)\frac{\Delta\sigma'}{E} \tag{7}$$

$$B = \frac{\Delta b_s}{b_o} = \left(\frac{s}{b_o} + \frac{a(1-\nu)}{b_o}\right)\varepsilon_s = \left(\frac{s}{b_o} + \frac{a(1-\nu)}{b_o}\right)\varepsilon_L \frac{P}{P + P_L} \tag{8}$$

where k is the new permeability, k_0 is the original permeability, b_0/a is the aspect ratio of pores, A represents the change in aperture due to poromechanical expansion, and B represents the reduction in aperture due to sorptive swelling. Eq. (6) can be rearranged as follows:

$$\left(\frac{k}{k_o}\right)^{\frac{1}{3}} = 1 + A - B \tag{9}$$

$$\left(\frac{k}{k_o}\right)^{\frac{1}{3}} + 1 = \sqrt[3]{(1+A)^3} + (1 - B) \tag{10}$$

$$(1-B)^3 = \left[\left(\frac{k}{k_o}\right)^{\frac{1}{3}} + 1 - \sqrt[3]{(1+A)^3}\right]^3. \tag{11}$$

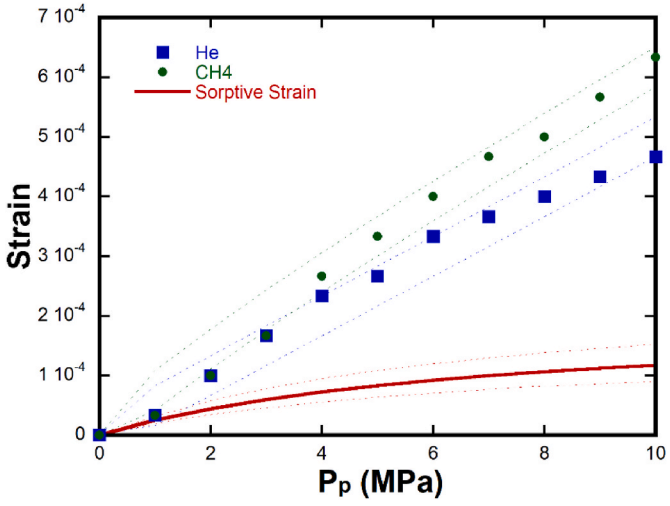

Fig. 5. Isolating the sorptive strain using Eq. (3) and Eq. (4). Subtracting the helium-induced strain data from the methane-induced strain data and fitting a Langmuir-type strain curve yields a Langmuir pressure P_L of 7 MPa and a Langmuir strain ε_L of 2.75×10^{-4}.

We note that $(1\text{-}B)^3$ is the permeability evolution in the absence of poromechanical expansion and $(1 + A)^3$ is the permeability evolution in the absence of Langmuir swelling. In Eq. (11), k/k_0 is the ensemble permeability response measured when using methane. In terms of the gases used in the experiments, we could cast Eq. (11) as follows:

$$\left(\frac{k}{k_o}\right)_{sorptive} = \left[\left(\frac{k}{k_o}\right)^{\frac{1}{3}}_{CH_4} + 1 - \left(\frac{k}{k_o}\right)^{\frac{1}{3}}_{He}\right]^3. \tag{12}$$

We plot the permeability data measured for helium and methane with increasing pore pressure in Fig. 6. The data are then used as input into Eq. (12) to show the signature of the sorption component of permeability evolution. Inputting the sorption data from Eq. (4) into Eq. (8) and using the observation that sorptive permeability loss is $(1\text{-}B)^3$ to convert Eq. (8) to the sorptive component of k/k_0, we then fit a curve to the data from Eq. (12) using s/b_0 equal to 1500 and b/a equal to 7×10^{-3}. In Fig. 6., the red curve represents the permeability reduction due to adsorptive pore closure predicted in Eq. (8) and the orange dots are the result of Eq. (12). We find an excellent fit and good agreement between these two independent methods of solving for sorptive strain and sorptive permeability evolution.

3.3. Nitrogen flooding results

In anticipation of permeability enhancement due to sorptive strain reduction, we model the expected result of nitrogen flooding at constant pore pressure in Fig. 7. Both Figs. 6 and 7 suggest an approximate doubling of permeability with methane desorption at 6 MPa pore pressure. After infiltrating the upstream side of a methane saturated core with nitrogen gas at constant pore pressure, we calculate permeability evolution using pressure pulse tests according to Eq. (1). We plot α/α_0 for each run, where α_0 is the pressure decay when the sample is 100% methane. We find that the value of α increases 79% in the bedding-parallel direction and 57% in the bedding-perpendicular direction. In order to convert this to permeability, we modify the Brace et al. (1968) equation to account for a simplified binary mixture:

$$k = f_i(\mu_i \beta_i)\frac{\alpha L}{A}\frac{V_{up}V_{dn}}{V_{up} + V_{dn}} \tag{13}$$

where

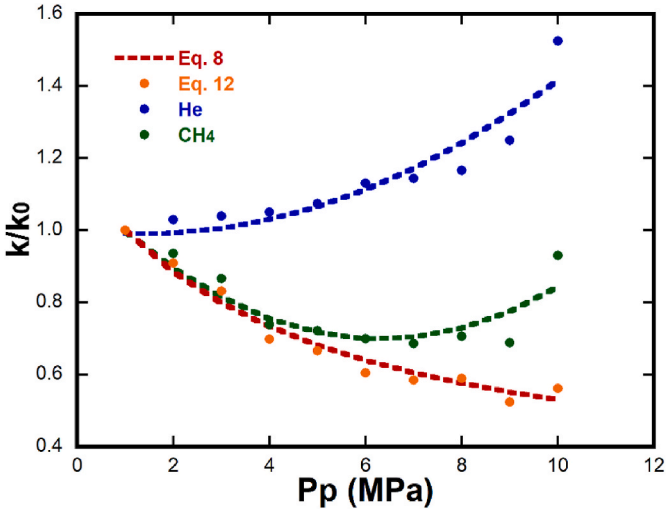

Fig. 6. Solving for sorptive permeability evolution for processes in parallel. Measurements are made with helium and methane. The isolated sorptive permeability from Eq. (12) is orange. The red curve is permeability loss calculating using aperture closure from Eq. (8). (For interpretation of the references to colour in this figure legend, the reader is referred to the Web version of this article.)

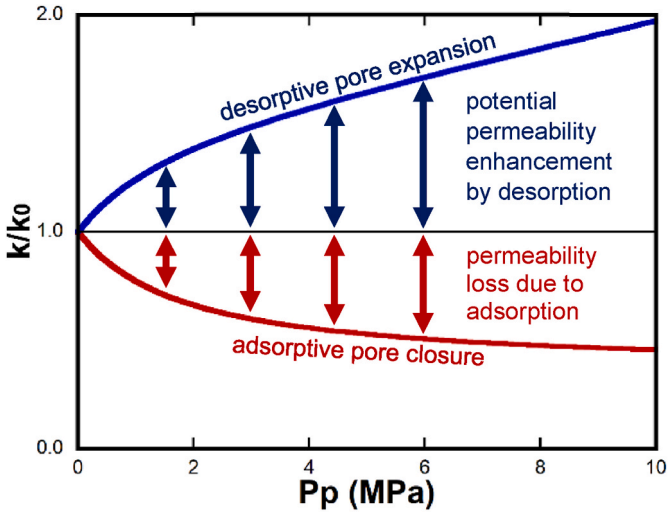

Fig. 7. Idealized permeability enhancement for a nitrogen flood at constant pore pressure. The blue curve is calculated by relaxing a sorptive strain on the order of 10^{-4} using the pore density and pore geometry calculated for Eq. (8). (For interpretation of the references to colour in this figure legend, the reader is referred to the Web version of this article.)

$$f_i = \frac{\alpha_n - \alpha_i}{\alpha_n - \alpha_1}. \tag{14}$$

Eq. (14) represents a simple interpolation scheme between two end points. The two variables that are not constant with changing mixture composition are the gas viscosity and gas compressibility. In our case, α_1 and α_n are the pressure decay when the sample is 100% methane and 100% nitrogen, respectively. The end point likely does not correspond with 100% nitrogen, but rather some irreducible methane saturation or a condition in which methane becomes entrained in the pore space. We find that the permeability increases 206% in the bedding-perpendicular sample and 222%–234% in the bedding-parallel samples. The bedding-perpendicular sample experienced less permeability enhancement, likely due to dominant flow paths being oriented orthogonal to gas flow. Results agree with the predicted permeability increase that should occur from relaxing the sorptive strain as seen in Fig. 6 and as illustrated in Fig. 7. The results for evolving α are plotted in Fig. 8 and the results for evolving permeability k are plotted in Fig. 9.

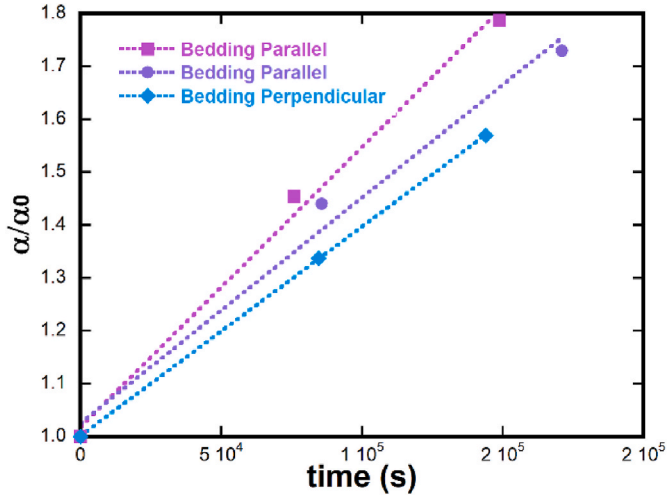

Fig. 8. Normalized pressure decay α/α_0. As N_2 infiltrates the sample, α increases.

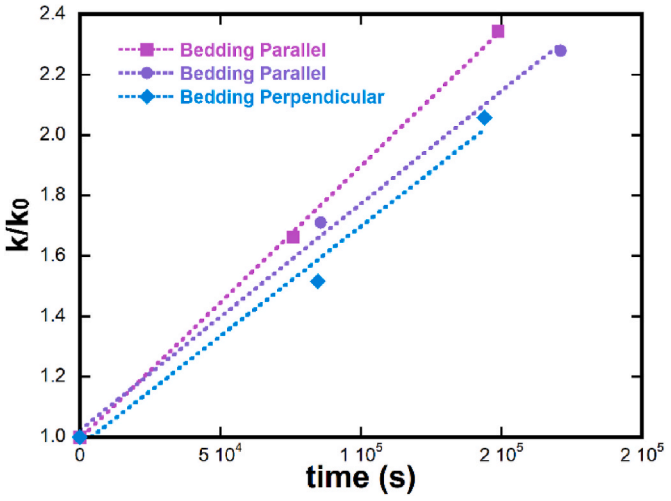

Fig. 9. Normalized permeability evolution k/k_0. Permeability increased 206% in the bedding-perpendicular sample and 222%–234% in the bedding-parallel samples.

4. Discussion

We examine the impacts of pore density, pore geometry, and sorptive strain on sorptive permeability evolution. Then we consider the mechanism by which organic matter shrinks during injection of nitrogen gas at constant pore pressure, which lowers the partial pressure of methane. Lastly, we consider alternative methods of sorption-driven permeability evolution and their potential for field application.

4.1. Pore density and pore geometry

In Eq. (8), the term s/b is the spacing-to-aperture ratio. In a two-dimensional model, s/b represents the length of shale matrix separating equally spaced pores. In shale matrix, the preferential flow paths created by bedding-parallel pores and micro-fissures are not uniformly spaced. Studies on larger systems show that flow paths of varying aperture and spacing can be averaged when contributing to flow in parallel, such as in our case examining the fissure-like pores oriented parallel to bedding (Narr, 1996; Ortega et al., 2006). We extend this concept of fracture density (b/s) for a parallel arrangement of fractures separated by matrix to approximate pore density – where the pores are necessarily elongate, as observed in shales. Large values of b/s correspond to a more dense distribution of fissure-like pores within the rock volume. For rocks with low pore density, strain is distributed over fewer pores that consequently experience greater pore closure (Schwartz et al., 2019b). Large s/b values indicate that each pore has to accommodate more of the sorptive strain than when pores are densely distributed. Permeability evolution in Eq. (8) matched an s/b value of approximately 1500, which suggests that sorptive permeability loss in shales is not driven primarily by the %TOC but rather by low pore density.

The term b/a is the aspect ratio, or pore geometry. Whereas s/b determines how much closure pores experience due to longitudinal strain, the pore geometry influences pore closure due to lateral strain. Flat pores are more mechanically compliant than circular pores. Flatter pores will experience greater permeability loss due to adsorption and greater permeability enhancement due to desorption. Fig. 10 shows an image of one of the Marcellus shale samples used in our experiments alongside an SEM image of the shale. The SEM image represents approximately 60 μm on each edge, showing porosity between grain boundaries ranging from nearly circular pores to flat cracks with low aspect ratios. In particular, microcracks responsible for preferential flow tend to follow grain boundaries and to have very low aspect ratios (Daigle et al., 2017). Fig. 10 also illustrates the concept of s/b as a ratio that characterizes the

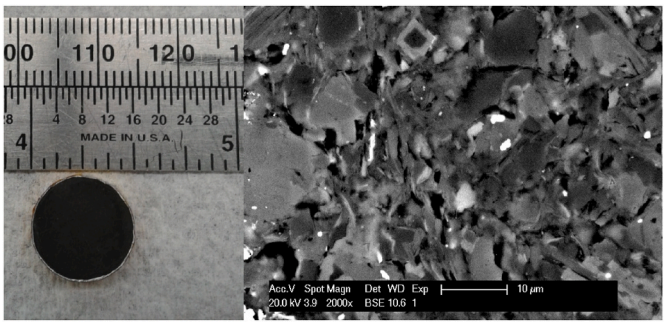

Fig. 10. Image of shale sample and SEM image at 2000× magnification.

distance between flow paths compared to the aperture of those same pores and cracks. Sorptive strains act homogenously in all directions with stresses modulated by restraint and anisotropic deformability. In a two-dimensional model with infinite planar fractures, sorptive strain occurring in the shale matrix between fractures does not cause any bulk expansion. Instead, the deformation is accommodated by fracture closure until maximum closure occurs. Since pores in shales do not have infinite length but rather are very small relative to the matrix surrounding them, the total amount of pore closure can be equated to the total bulk expansion.

The longitudinal component of the sorptive strain is measured with an LVDT and represents the additional expansion caused by increasing pore pressure with a sorptive gas. This same strain is then used to calculate pore closure, allowing the possibility that the sorptive strain is double counted in our model. The constraint that pore length a is very small compared to the distance between pores resolves this issue. If there is ample space between pores along the same horizontal bedding plane, the sorptive swelling within those spaces will cause the material to expand by the same amount as pores are closing.

By using an LVDT mounted along the axial direction of the core, we measure the longitudinal component of the sorptive strain. The volumetric sorptive strain would be approximately two to three times larger, depending on the degree of anisotropy in the shale. The longitudinal strain is chosen because of the dominant permeability that shales exhibit in the bedding-parallel direction. As preferential flow paths run through the porosity concentrated between laminae, expansion and deformation perpendicular to the flow paths cause a direct change in pore aperture. A shortening of length that is parallel to these flow paths has a negligible impact on permeability evolution, and in such a case a three-dimensional model collapses to the two-dimensional model proposed here. For rocks with low values of permeability anisotropy volumetric strain may be a more appropriate parameter.

4.2. Lowering the partial pressure of methane causes desorption

In the case of nitrogen flooding at constant pore pressure, there is no additional poromechanical expansion in the pore space to enhance permeability. The only changing strain within the matrix is the shrinkage of the organic matter as methane desorbs. The mechanism by which nitrogen induces desorption is by lowering the partial pressure of the methane while maintaining the overall pore pressure. The swelling caused by the methane adsorption is relaxed and flow channels become less constricted. The small pressure differential at either end of the sample—which is ± 0.3 MPa—allows for movement of gas within the sample from the upstream to the downstream side. However, this is not the same mechanism as increasing the pore pressure within the sample itself—certainly there is a pressure gradient within the sample, but that same gradient exists when taking the original methane permeability measurements and is necessary to conduct pressure pulse tests. Identical circumstances—a core saturated with gas at 6 MPa pore pressure with a ± 0.3 MPa differential at the inlet and outlet in order to allow for fluid flow—exists in both the methane and nitrogen measurements.

Permeability models for multicomponent gas mixtures have been developed for coals (Mavor and Gunter, 2004). While an extended Langmuir equation for binary mixtures could be used (Wu et al., 2011), the primary mechanism responsible for the sorptive strain evolution is desorption due to decreasing partial pressure of methane. This allows for a simple model to be developed that only has to account for the sorptive strain caused by the sorptive species. While nitrogen is slightly sorptive, it has been shown to generate less than one-fifth the sorptive strain in coals with very high %TOC (Chen et al., 2012) and we treat it as non-sorptive for shales. If the sorptive strain at a given pore pressure is known, then potential permeability enhancement is

$$\frac{k}{k_o} = \left(1 + \left(\frac{s}{b_o} + \frac{a(1-\nu)}{b_o}\right)\varepsilon_s\right)^3 \tag{15}$$

where sorptive strain is added to account for increasing aperture instead of subtracted as in Eq. (6) which accounted for permeability loss.

4.3. Alternative methods

The Langmuir strain is independent of temperature for each gas species but does change based on the sorption affinity of each gas species (Robertson and Christiansen, 2007; Singh and Cai, 2018). In the present study, we focus on methane, nitrogen and helium; however, the impacts of carbon dioxide injection should be mentioned. Whereas carbon dioxide has a stronger affinity to adsorb than methane, nitrogen is a very weakly sorptive gas. Indeed, it can be treated as a non-sorptive gas when compared to methane adsorption in shales. CO_2 injection into a methane saturated shale causes desorption of methane by preferential adsorption of CO_2. The CO_2 has a higher affinity to adsorb in the organic pore space of coals and shales, leading to more storage, larger sorptive strains, and greater permeability loss (Li and Elsworth, 2015; Chareonsuppanimit et al., 2012). The additional permeability loss would be based on the partial pressure of each species and the difference between the Langmuir strains of methane and carbon dioxide.

While N_2 flooding may increase methane recovery by increasing matrix permeability, CO_2 is more sorptive than methane and causes more swelling of the organic material at a given pore pressure. Adsorption of CO_2 lowers permeability but also increases methane recovery as the native methane is desorbed into the free gas phase (Pan and Connell, 2012; Liu et al., 2017). We suggest further study comparing these two gases to determine which of these competing mechanisms—permeability enhancement due to shrinking of the organic material and increased methane production due to preferential adsorption of CO_2—has a larger impact on ultimate recovery.

5. Conclusions

We have shown that the component of permeability evolution due to sorptive swelling can be isolated. We have developed a model that uses the isolated sorptive strain to predict permeability evolution due to sorptive gas species. Sorptive swelling can be relaxed at constant pore pressure to recover permeability by an amount predicted by the model. Shales can experience sorptive permeability loss similar to coals because of their low pore density.

The matrix permeability of a shale can be increased two-fold by nitrogen flooding. Laboratory results show a 206% and a 234% permeability increase in the bedding-perpendicular and bedding-parallel directions, respectively. For the case of nitrogen flooding conducted at near-constant pore pressure considered here, the sorption induced permeability reduction and sorptive strain can be isolated in order to determine the possible permeability enhancement that could be caused by methane desorption.

The magnitude of permeability enhancement that will result is strongly dependent on the pore density in the matrix: high s/b ratios

experience larger permeability enhancements than smaller *s/b* ratios. The pore geometry creates a similar consideration: flat pores are more geometrically compliant and will experience greater permeability loss at any magnitude of organic swelling than circular pores which are stiffer. These two considerations in part explain how shales often experience similar permeability evolution to coals which have much larger %TOC. On the other hand, our results may not be valid for all shale types. Care should be taken to characterize the mineralogy, mineral distribution, sorptive capacity, sorptive strain, location of flow paths relative to sorptive components, pore geometry, pore stiffness relative to matrix stiffness, and spacing between pores in order to determine if a shale type would experience the same magnitude of permeability enhancement as seen here.

A limitation of the analysis in this study is that concentrations of nitrogen and methane throughout the experiment could not be directly measured within the core. However, the final permeability enhancement corresponds to either 100% nitrogen or, more likely, to an irreducible methane concentration. Therefore, values of $\alpha\ (= ln(dp)/dt)$ in pressure pulse tests can be used to interpolate relative concentrations of binary mixtures with reasonable accuracy such that mixture viscosity and compressibility can be adjusted to produce a measurement of permeability. We also recommend measuring the pore surface area and pore size distribution in future studies. Combined with mineralogy data including clay content and %TOC, these measurements can provide valuable insights into the surface area available for gas adsorption and the resulting magnitude of the sorptive strain. Pore size distribution can also be used to quantify pore structure and geometry, which can further constrain permeability models for improved characterization of sorption-driven permeability evolution.

Author statement

The manuscript “Sorptive permeability loss determined from strain-based analysis of tightly constrained experiments on shale” is a dual-author study performed by Brandon Schwartz and Derek Elsworth. Brandon Schwartz was responsible for the planning, execution, synthesis, and writeup of the manuscript. Derek Elsworth was responsible for the planning, supervision, and writeup of the manuscript.

Declaration of competing interest

The authors declare no competing interests associated with this publication.

Acknowledgements

This work is a partial result of support from Chevron Energy Technology Company, and their support is gratefully acknowledged.

References

Bandyopadhyay, K., 2009. Seismic Anisotropy: Geological Causes and its Implications to Reservoir Geophysics. Stanford University.
Brace, W., Walsh, J.B., Frangos, W.T., 1968. Permeability of granite under high pressure. J. Geophys. Res. 73 (6), 2225–2236.
Bonnelye, A., Schubnel, A., David, C., Henry, P., Guglielmi, Y., Gout, C., Dick, P., 2017. Elastic wave velocity evolution of shales deformed under uppermost crustal conditions. J. Geophys. Res. Solid Earth 122 (1), 130–141.
Chareonsuppanimit, P., Mohammad, S.A., Robinson Jr., R.L., Gasem, K.A., 2012. High-pressure adsorption of gases on shales: measurements and modeling. Int. J. Coal Geol. 95, 34–46.
Chen, Z., Liu, J., Pan, Z., Connell, L.D., Elsworth, D., 2012. Influence of the effective stress coefficient and sorption-induced strain on the evolution of coal permeability: model development and analysis. Int. J. Greenh. Gas Control 8, 101–110.
Crook, A.J., Yu, J.G., Willson, S.M., 2002. Development of an orthotropic 3D elastoplastic material model for shale. In: SPE/ISRM Rock Mechanics Conference. Society of Petroleum Engineers.
Cui, X., Bustin, R.M., 2005. Volumetric strain associated with methane desorption and its impact on coalbed gas production from deep coal seams. AAPG (Am. Assoc. Pet. Geol.) Bull. 89 (9), 1181–1202.
Daigle, H., Hayman, N.W., Kelly, E.D., Milliken, K.L., Jiang, H., 2017. Fracture capture of organic pores in shales. Geophys. Res. Lett. 44 (5), 2167–2176.
Harpalani, S., Schraufnagel, R.A., 1990. Influence of matrix shrinkage and compressibility on gas production from coalbed methane reservoirs. In: SPE Annual Technical Conference and Exhibition. Society of Petroleum Engineers.
Harpalani, S., Chen, G., 1997. Influence of gas production induced volumetric strain on permeability of coal. Geotech. Geol. Eng. 15 (4), 303–325.
Heng, S., Li, X., Liu, X., Chen, Y., 2020. Experimental study on the mechanical properties of bedding planes in shale. J. Nat. Gas Sci. Eng. 76, 103161.
Izadi, G., Wang, S., Elsworth, D., Liu, J., Wu, Y., Pone, D., 2011. Permeability evolution of fluid-infiltrated coal containing discrete fractures. Int. J. Coal Geol. 85 (2), 202–211.
Keller, L.M., Holzer, L., Wepf, R., Gasser, P., 2011. 3D geometry and topology of pore pathways in Opalinus clay: implications for mass transport. Appl. Clay Sci. 52 (1–2), 85–95.
Kumar, H., Elsworth, D., Mathews, J.P., Marone, C., 2016. Permeability evolution in sorbing media: analogies between organic-rich shale and coal. Geofluids 16 (1), 43–55.
Levine, J.R., 1996. Model study of the influence of matrix shrinkage on absolute permeability of coal bed reservoirs. Geological Society, London, Special Publications 109 (1), 197–212.
Li, X., Elsworth, D., 2015. Geomechanics of CO2 enhanced shale gas recovery. J. Nat. Gas Sci. Eng. 26, 1607–1619.
Li, X., Feng, Z., Han, G., Elsworth, D., Marone, C., Saffer, D., Cheon, D., 2017. Permeability evolution of propped artificial fractures in Green River shale. Rock Mech. Rock Eng. 50 (6), 1473–1485.
Liu, H.H., Rutqvist, J., 2010. A new coal-permeability model: internal swelling stress and fracture–matrix interaction. Transport Porous Media 82 (1), 157–171.
Liu, J., Chen, Z., Elsworth, D., Qu, H., Chen, D., 2011. Interactions of multiple processes during CBM extraction: a critical review. Int. J. Coal Geol. 87 (3–4), 175–189.
Liu, J., Chen, Z., Elsworth, D., Miao, X., Mao, X., 2010. Linking gas-sorption induced changes in coal permeability to directional strains through a modulus reduction ratio. Int. J. Coal Geol. 83 (1), 21–30.
Liu, J., Yao, Y., Liu, D., Elsworth, D., 2017. Experimental evaluation of CO2 enhanced recovery of adsorbed-gas from shale. Int. J. Coal Geol. 179, 211–218.
Lu, X.C., Li, F.C., Watson, A.T., 1995. Adsorption measurements in Devonian shales. Fuel 74 (4), 599–603.
Lyu, Q., Ranjith, P.G., Long, X., Kang, Y., Huang, M., 2015. Effects of coring directions on the mechanical properties of Chinese shale. Arabian J. Geosci. 8 (12), 10289–10299.
Mavor, M.J., Vaughn, J.E., 1998. Increasing coal absolute permeability in the San Juan Basin fruitland formation. SPE Reservoir Eval. Eng. 1 (3), 201–206.
Mavor, M.J., Gunter, W.D., 2004. Secondary porosity and permeability of coal vs. gas composition and pressure. In: SPE Annual Technical Conference and Exhibition. Society of Petroleum Engineers.
Mazumder, S., Wolf, K.H., 2008. Differential swelling and permeability change of coal in response to CO2 injection for ECBM. Int. J. Coal Geol. 74 (2), 123–138.
Narr, W., 1996. Estimating average fracture spacing in subsurface rock. AAPG (Am. Assoc. Pet. Geol.) Bull. 80 (10), 1565–1585.
Ortega, O.J., Marrett, R.A., Laubach, S.E., 2006. A scale-independent approach to fracture intensity and average spacing measurement. AAPG (Am. Assoc. Pet. Geol.) Bull. 90 (2), 193–208.
Palmer, I., Mansoori, J., 1996. How permeability depends on stress and pore pressure in coalbeds: a new model. In: SPE Annual Technical Conference and Exhibition. Society of Petroleum Engineers.
Palmer, I., 2009. Permeability changes in coal: analytical modeling. Int. J. Coal Geol. 77 (1–2), 119–126.
Pan, Z., Connell, L.D., 2012. Modelling permeability for coal reservoirs: a review of analytical models and testing data. Int. J. Coal Geol. 92, 1–44.
Robertson, E.P., 2008. *Improvements In Measuring Sorption-Induced Strain and Permeability in Coal* (No. INL/CON-08-14637). Idaho National Laboratory (INL).
Robertson, E.P., Christiansen, R.L., 2006. *A Permeability Model for Coal and Other Fractured, Sorptive-Elastic Media* (No. INL/CON-06-11830). Idaho National Laboratory (INL).
Robertson, E.P., Christiansen, R.L., 2007. Modeling laboratory permeability in coal using sorption-induced strain data. SPE Reservoir Eval. Eng. 10 (3), 260–269.
Robertson, E.P., 2005. Measurement and Modeling of Sorption-Induced Strain and Permeability Changes in Coal. United States. Department of Energy.
Sakhaee-Pour, A., Bryant, S., 2012. Gas permeability of shale. SPE Reservoir Eval. Eng. 15 (4), 401–409.
Schwartz, B., Elsworth, D., Marone, C., 2019a. Relationships between mechanical and transport properties in Marcellus shale. Int. J. Rock Mech. Min. Sci. 119, 205–210.
Schwartz, B., Huffman, K., Thornton, D., Elsworth, D., 2019b. A strain based approach to calculate disparities in pore structure between shale basins during permeability evolution. J. Nat. Gas Sci. Eng. 68, 102893.
Schwartz, B., Huffman, K., Thornton, D., Elsworth, D., 2019c. The effects of mineral distribution, pore geometry, and pore density on permeability evolution in gas shales. Fuel 257, 116005.
Seidle, J.P., Jeansonne, M.W., Erickson, D.J., 1992. Application of matchstick geometry to stress dependent permeability in coals. In: SPE Rocky Mountain Regional Meeting. Society of Petroleum Engineers.
Shi, J.Q., Durucan, S., 2005. A model for changes in coalbed permeability during primary and enhanced methane recovery. SPE Reservoir Eval. Eng. 8 (4), 291–299.
Singh, H., Cai, J., 2018. A mechanistic model for multi-scale sorption dynamics in shale. Fuel 234, 996–1014.

Sone, H., Zoback, M.D., 2013. Mechanical properties of shale-gas reservoir rocks—Part 1: static and dynamic elastic properties and anisotropy. Geophysics 78 (5), D381–D392.
Siriwardane, H., Haljasmaa, I., McLendon, R., Irdi, G., Soong, Y., Bromhal, G., 2009. Influence of carbon dioxide on coal permeability determined by pressure transient methods. Int. J. Coal Geol. 77 (1–2), 109–118.
Wang, S., Elsworth, D., Liu, J., 2012. A mechanistic model for permeability evolution in fractured sorbing media. J. Geophys. Res. Solid Earth 117 (B6).
Wu, Y., Liu, J., Chen, Z., Elsworth, D., Pone, D., 2011. A dual poroelastic model for CO2-enhanced coalbed methane recovery. Int. J. Coal Geol. 86 (2–3), 177–189.
Yan, C., Deng, J., Hu, L., Chen, Z., Yan, X., Lin, H., Tan, Q., Yu, B., 2015. Brittle failure of shale under uniaxial compression. Arabian J. Geosci. 8 (5), 2467–2475.
Zhang, H., Liu, J., Elsworth, D., 2008. How sorption-induced matrix deformation affects gas flow in coal seams: a new FE model. Int. J. Rock Mech. Min. Sci. 45 (8), 1226–1236.